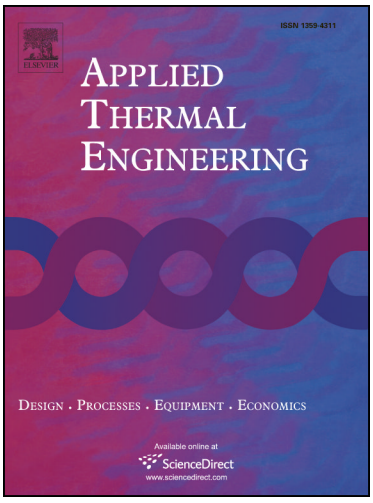

Two-dimensional approach for the numerical simulation of large bore reciprocating compressors thermodynamic cycle

Francesco Balduzzi, Andrea Tanganelli, Giovanni Ferrara, Alberto Babbini

PII: S1359-4311(17)32702-3
DOI: https://doi.org/10.1016/j.applthermaleng.2017.10.041
Reference: ATE 11239

To appear in: *Applied Thermal Engineering*

Received Date: 21 April 2017
Revised Date: 13 September 2017
Accepted Date: 8 October 2017

Please cite this article as: F. Balduzzi, A. Tanganelli, G. Ferrara, A. Babbini, Two-dimensional approach for the numerical simulation of large bore reciprocating compressors thermodynamic cycle, *Applied Thermal Engineering* (2017), doi: https://doi.org/10.1016/j.applthermaleng.2017.10.041

Two-dimensional approach for the numerical simulation of large bore reciprocating compressors thermodynamic cycle

Francesco Balduzzi[1*], Andrea Tanganelli[1], Giovanni Ferrara[1], Alberto Babbini[2]

[1] *Department of Industrial Engineering, University of Florence - Via di Santa Marta 3, 50139, Firenze, Italy - Tel. +39 055 2758773 - Fax +39 055 2758755 - balduzzi@vega.de.unifi.it*

[2] *GE Oil & Gas - Via F. Matteucci 2, 50127, Firenze, Italy - Tel. +39 055 4232587 - Fax +39 055 4232800 - alberto.babbini@ge.com*

[*] *= contact author*

Research highlights

- 2D CFD simulations compared to experimental data on a reciprocating compressor
- Novel method for a 2D numerical model for the analysis of the thermodynamic cycle
- Use of porous simplification for valves and plenums modeling
- Predictability is enhanced with respect to low order models

Abstract

The performance of large reciprocating compressors is strongly dependent on the geometry of gas chambers and valve pockets, both directly influencing the pressure losses along the flow path. Reliable and accurate numerical models are necessary for a proper prediction of the thermodynamic cycle of the compressor, hence of both the efficiency and the absorbed power. In order to account for the effect of the geometrical features, the detail level of the modeling technique needs to be suitable for capturing the most significant phenomena related to the physics involved. To this end, CFD simulations can represent a viable tool for the analysis of the working cycle. Due to the complexity of the geometry and the large extent of the fluid domain, unsteady three-dimensional CFD simulations are very demanding in terms of computational resources, resulting in unreasonably lengthy simulations and specialized hardware requirements.

The present paper describes a two-dimensional CFD modelling strategy aimed at reducing the computational effort by ensuring a compromise between the accuracy of the results and the simulation costs. A simplified geometry is used to allow the reduction of the three-dimensional fluid domain to an equivalent two-dimensional representation. The suitability of using two-dimensional models for the numerical simulation of the thermodynamic cycle of large reciprocating compressors is analyzed and discussed. In the paper, the simulation results of a double-acting large bore cast iron cylinder are compared to experimental measurements. A satisfactory agreement was obtained when comparing the

numerical data to the measurements of dynamic pressure sensors placed in the cylinder head, clearance volume adjustment plugs and suction and discharge nozzles. A comparison with the simulation results of low-order numerical models is also shown to highlight the enhancement in the performance predictability.

The matching between experimental and simulated results, together with the short calculation time, confirms the high potential of the proposed solution in predicting the expected performance of the machine, in terms of indicated power and specific work. Moreover, additional benefits are related to the possibility of investigating the pressure oscillations and distributions in the cylinder chambers, and the mass flow rates for the analysis of the suction and discharge pipelines.

Keywords

Reciprocating compressor, CFD, 2D modeling, working cycle, porous medium

Nomenclature

Latin symbols

A_t	pocket throat section	[m]
B	cylinder bore	[m]
BDC	Bottom Dead Center	
c	head clearance	[m]
CFD	Computational Fluid Dynamics	
D	permeability coefficient	[m^{-2}]
D_v	valve diameter	[m]
F	resistance coefficient	[m^{-1}]
FVM	Finite Volume Method	
H_c	cylinder height	[m]
H_m	masking height	[m]
H_p	pocket height	[m]
k	turbulence kinetic energy	[m^2/s^2]
Ks_v	valve flow coefficient	[-]
Ks_p	plenum flow coefficient	[-]
L_p	pocket length	[m]
L_s	slide length	[m]
p	pressure	[Pa]
p^*	dimensionless pressure	[-]
R^2	coefficient of determination	[-]
S	stroke	[m]
t	pocket throat	[m]
TDC	Top Dead Center	
V	velocity	[m/s]
x	piston position	[m]

Greek symbols

β_s	slide angle	[deg]
ϑ	crank-angle	[deg]
ε	turbulence dissipation date	[m^2/s^3]
μ	viscosity	[Kg/m/s]
ρ	density	[kg/m^3]

1. Introduction

The thermodynamic cycle of a large reciprocating compressor is largely influenced by the fluid-dynamic phenomena occurring along the overall flow path of the machine. In particular, the differences between the real working cycle and the ideal cycle are mainly related to the gas pressure drop due to friction losses, the pulsating flow within inlet and outlet manifolds and the heat transfer through solid walls. Therefore, a numerical model capable of accounting for all of these effect is required for an accurate prediction of the absorbed power.

Although the highest accuracy can be achieved with three-dimensional CFD analyses, the fluid dynamics consisting of both flow complexity, large domain extent and unsteady behavior is challenging and has discouraged high-level fluid-dynamic studies. The work of Traversari et al. [1] is an example of transient 3D CFD simulation, in which a fluid structure interaction analysis was performed with the aim to simulate the thermodynamic cycle of a reciprocating compressor by computing also the valve rings motion according to the fluid drag forces. However, the need of high performance hardware and large computational time makes this approach unsuitable as a general design tool. Three-dimensional simulations are preferred for the investigation of more specific aspects, such as the interaction between the piston motion and the effective flow inside a discharge valve, as shown by Pereira et al. [2].

In the current literature, the use of lumped parameter models is the most common approach for predicting the compressor performance. They are suitable for preliminary analysis thanks to the low computational cost. The compressor chamber is modeled as a time-dependent 0D element, therefore the thermodynamic properties are uniform in the whole fluid domain and the change of state in the cylinder chamber follows quasi-static transformations. Since it is well known that the automatic valve is the most crucial component, related both to the largest contribution to the pressure losses and to its complex dynamic motion, the mass flow is computed by taking into account the valve flow coefficient (Ks_v). Costagliola [3] developed a model accounting also for the valve dynamics, which was used also by Winandy et al. [4] and Elhaj et al. [5] for the estimation of compressor performance. Yang et al. [6] introduced also the effects leakage and frictions for the analysis of a semi-hermetic CO_2 reciprocating compressor. In all of these studies, the numerical results were compared with experimental data, showing that such approach is suitable for preliminary evaluations but the prediction of the compression cycle is not always satisfactory.

Moreover, all of the other components along the suction and discharge gas chambers play a key role and are not always accurately accounted for. In common practice, these losses are often accounted for by using empirical correlations to correct the valve flow coefficient, as proposed by Bauer [7] and used by Boeswirth et al. [8] and Machu [9].

Some of the authors proposed a novel methodology based on steady-state 3D CFD simulations to define a flow coefficient (Ks_p) of the pocket-plenum system ([10,11]). The approach is based on a simplification of the computational domain by substituting the valve geometry with an equivalent porous medium that generates a localized pressure drop equivalent to the actual valve. Its applicability has been shown in [12], where a hybrid time-frequency domain lumped parameter model, developed by Stiaccini et al. ([13,14]), was used for the analysis of the influence of the valve retainer orientation on the performance of a reciprocating compressor. To further increase the complexity of lumped parameter models, the pressure waves' propagation, which controls the filling of the cylinder, can be characterized by a one-dimensional unsteady compressible approach for the external ducts. Gimelli et al. [15] compare the computed mass flow rates of a 0D-1D simulation with measured values showing a good agreement between results.

Dealing with large reciprocating compressors, the combination of the low revolution speed with the extent of the cylinder bore leads to additional effects that need to be accounted for in the numerical model. It can be observed that the time needed for the pressure waves to travel the whole cylinder bore is comparable with the duration of the physical phenomena of the thermodynamic cycle. A 0D representation of the compression chamber is not appropriate for an accurate prediction of the gas transfer process during the suction and discharge phases. To overcome this limitation, a spatial discretization of the compression chamber domain is necessary to simulate the gas motion inside the cylinder. The effect of waves and unsteady flow conditions inside the cylinder was studied by Machu in [16] by using the method of characteristics. In further works ([17,18]), Machu developed a numerical model based on the one dimensional Euler equations to describe also laterally running waves. Aigner developed in [19] a compressor model with a spatial discretization both for the cylinder chamber and for the compressor plenums. Some of the authors developed a 1D numerical model [20] based on the Finite Volume Method (FVM). The discretization is applied in the valve-to-valve direction since the flow inside the compression chamber has a preferential direction, being the axes of suction and discharge valves orthogonal to the cylinder axis. The enhanced prediction capability was demonstrated by comparing the computed working cycle of both the 1D FVM model and a lumped parameter model with the experimental data collected on a dedicated test bench for a double-acting cast iron cylinder.

The goal of the present activity is to define a methodology to perform a 2D CFD simulation of the working cycle of a reciprocating compressor in order to provide more accurate results than low-order models and, at the same time, to guarantee the reduction of the computational effort with respect to unsteady 3D CFD simulations. In more detail, the analyses presented this paper were carried out for the double-acting large bore cast iron cylinder of ref. [20]. The simplifications required to allow the reduction of the three-dimensional fluid domain to an equivalent two-dimensional configuration are shown. The suitability of using two-dimensional models for the numerical simulation of the thermodynamic cycle of large reciprocating compressors is analyzed and discussed. The matching between experimental and simulated results, together with the short calculation time, confirms the high potential of the proposed solution in predicting the expected performance of the machine, in terms of indicated power and specific work. Moreover, additional benefits are related to the possibility of investigating the pressure oscillations and distributions in the cylinder chambers, and the mass flow rates for the analysis of the suction and discharge pipelines.

2. Case study

The 2D CFD numerical model was used to simulate the working cycle of a real compressor that works with pure nitrogen (N_2) as working fluid. The main characteristics and the operating conditions of the water-cooled double-acting cast iron cylinder with a bore of 770 mm are summarized in Table 1.

Table 1 – Compressor specifications: geometry and operating conditions.

Parameter	Units	Value
Bore	[mm]	770
Stroke	[mm]	360
Dead volume	[%]	12
# Suction Valves	[-]	3 + 3
# Discharge Valves	[-]	3 + 3
Rotating speed	[rev/min]	375

Numerical results were compared with measurements collected at the test bench during an experimental campaign on the compressor.

Experiments have been conducted on the compressor at full load conditions at a rotating speed of 375 rev/min. The head end of the cylinder, whose geometry is depicted in Figure 1 (a), was equipped with multiple dynamic pressure sensors for monitoring the compressor operation, as shown in Figure 1 (b). The pressure in the compression chamber was monitored using a pressure sensor located in the center of the head (P_H). Three sensors are used to monitor the suction valves head pressure (P_{S1}, P_{S2}, P_{S3}), three for the discharge valves head pressure (P_{D1}, P_{D2}, P_{D3}) and two sensors for the suction and discharge nozzles (P_{N1}, P_{N2}).

Figure 2 shows the experimental data collected as a function of the piston position, where the values of pressure are reported in a dimensionless form (p^*), normalized by the suction pressure (p_s) and the discharge pressure (p_d) as follows:

$$p^* = \frac{p - p_s}{p_d - p_s} \tag{1}$$

Therefore, $p^*=0$ corresponds to the suction pressure and $p^*=1$ corresponds to the discharge pressure. In the figure, the curves representing the pressure trend in both suction and discharge valves refer to the central valve.

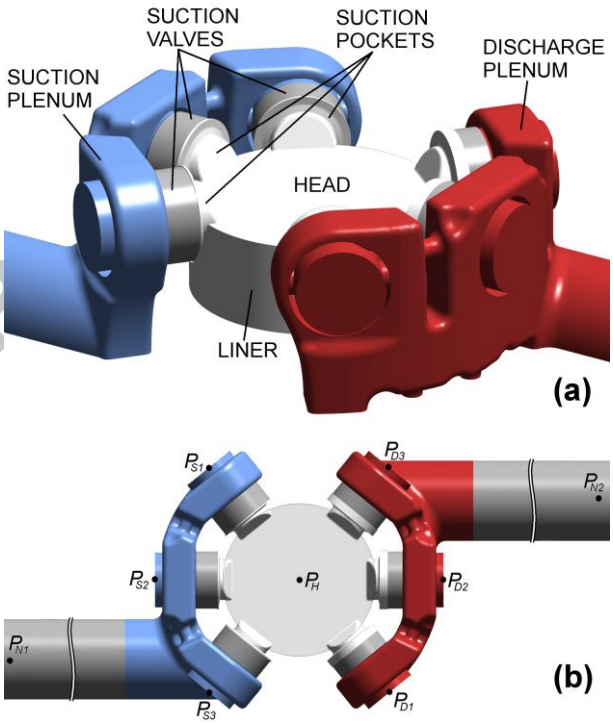

Figure 1 – Fluid-dynamic domain of the cylinder's head-end (a) and locations of the pressure sensors (b).

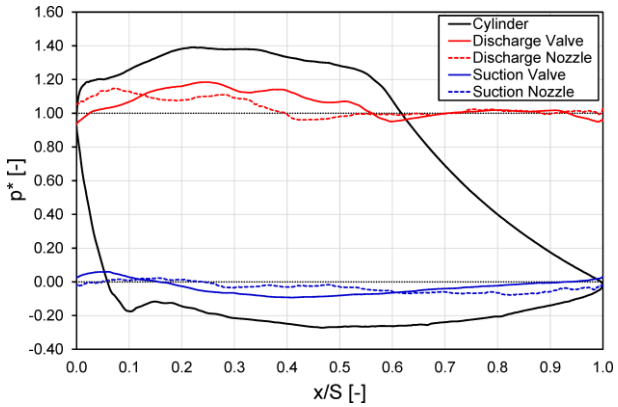

Figure 2 – Experimental diagram of the working cycle.

3. CFD model

Beyond any doubt, the three-dimensional approach is the only able to really describe the actual functioning of the machine. The valves orientation, the valve-retainer geometry and the complexity of the plenum shape impose to the fluid flow to follow a strongly three-dimensional path. Notwithstanding this, the development of a robust transient 3D CFD approach requires unreasonably lengthy simulations and large computational resources, due to the huge extension of the overall fluid domain. On the other hand, lumped parameter models, which are the easiest models to implement, fail to correctly predict the working cycle. One-dimensional models are thought to be the best compromise in terms of accuracy of the prediction and computational costs and complexity. However, they require a much greater effort from the point of view of the numerical implementation since no dedicated software is available. In any case, both lumped parameter and 1D models require the knowledge of valve flow coefficient (Ks_v), as well as the pocket and plenum flow coefficient (Ks_p).

Therefore, the goal was to define an approach ensuring the best compromise between performance predictability, computing effort and programming of numerical code.

The computational resources required for a 2D simulation are compatible with the requirements in the design phase, although much higher in comparison to low-order models. Notwithstanding this, the main advantage is the possibility of using general purpose commercial or open-source CFD codes, thus avoiding the need of writing and implementing an in-house FVM software. Within these preconditions, the authors investigated the potential of a 2D simulation strategy in enhancing the predictability of the thermodynamic cycle of reciprocating compressors.

3.1 2D strategy

The first step for the definition of the 2D model is the transformation from the original 3D geometry into an equivalent 2D representation. The strategy adopted for the reduction of all of the 3D regions is different, depending on the three-dimensional features of the various geometric parts. Indeed, only the 3D properties that affect the working cycle have to be accounted for. In particular, valves and plenums are characterized by very complex 3D paths, which are not trivial to reduce to 2D. Moreover, their effect on the working cycle is mainly related to the pressure drop resulting from the flow of the gas during the suction on discharge phases. To overcome this criticality, some of the authors proposed in the recent past a novel methodology for the evaluation of the pressure losses occurring along the overall gas path [10]. The methodology is based on a simplified CFD approach in which the valve geometry is

replaced with an "equivalent" porous medium. The porous model is specifically calibrated to generate a localized pressure drop equivalent to the actual valve.

In the present activity, an extension of the proposed methodology to transient simulations for the working cycle prediction is shown. The fluid volumes of valves and plenums are treated as porous mediums, without the need of a detailed geometrical characterization. In this way, the same fluid-dynamic parameters (Ks_v and Ks_p) used in low-order models are adopted. The benefit is a reduction both in the runtime and in the time required for setting up the model, without significantly affect the predictability of the absorbed power. As a result, the fluid domain is decomposed in seven separate regions, as shown in Figure 3. The plenums and valves regions are simply modeled as rectangular porous regions with the purpose of replicating the main effect of the actual geometry on the flow, i.e., the same pressure drop.

Also the reduction of the compression chamber volume requires a special treatment. When dealing with large size reciprocating compressors, the flow inside the cylinder has a preferential direction, i.e. the flange-to-flange direction. The results of the 1D FVM model shown in ref. [20] revealed that a discretization of the compression chamber volume along the diametrical axis connecting suction and discharge central valves is suitable to catch the main phenomena of pressure wave propagation and mass flow of gas inside the cylinder. For the 2D representation of the cylinder, the second dimension was added in the direction of the cylinder axis, since the flow is strongly guided by the valve pocket shape and by the interaction with the moving piston. The transversal direction is therefore neglected, suppressing directional effects caused by lateral valves, which anyhow are deemed to be of secondary relevance.

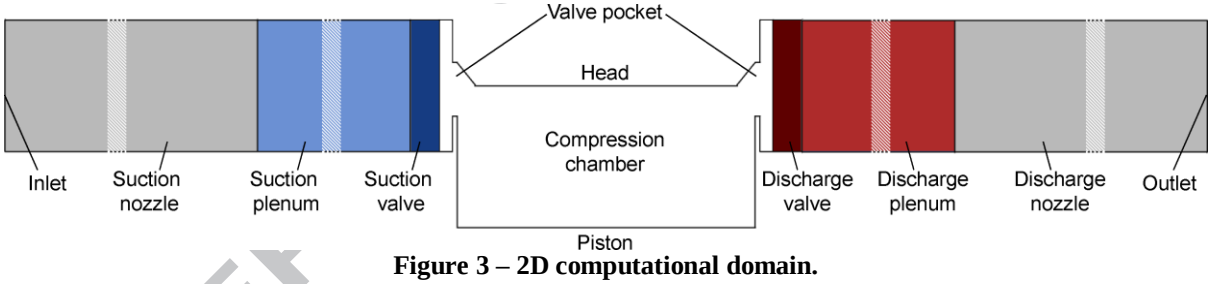

Figure 3 – 2D computational domain.

As a result, the geometry of the cylinder and the valve pockets (Figure 4) is modeled through a simplified 2D representation in the plane containing the cylinder axis and parallel to the flanges axes, defined by the following features:

- The cylinder is reduced to a rectangular area, defined by the cylinder bore (B) and the cylinder height (H_c), defined as the sum of the piston stroke (S) and the clearance (c) between the piston and the head at the Top Dead Center (TDC);
- For both suction and discharge geometries, the three valve pockets are reduced to a single equivalent pocket defined by two critical cross-section: the pocket throat (t) and the pocket height (H_P). Both cross sections are computed by imposing the same ratio of the actual flow sections, as reported in Eq. 2 and Eq. 3:

$$\frac{H_P}{B} = \frac{3\frac{\pi D_v^{\,2}}{4}}{\frac{\pi B^2}{4}} \qquad (2)$$

$$\frac{t}{B} = \frac{3A_t}{\frac{\pi B^2}{4}} \tag{3}$$

where D_v is the valve diameter and A_t is the throat area of the three-dimensional pocket. The angle (β_s) and the length (L_s) of the slide due to the machining on the cylinder head are analogous to the actual ones. Due to the 2D approximation, the constraint on the pocket throat does not allow to preserve the angle when the piston starts the masking of the window of the valve pocket, since the masking height is not preserved.

- The pocket length (L_P) is computed in order to guarantee the same volumetric compression ratio, i.e. the area at TDC is equal to 12% of the displacement ($B \times S$ in the 2D case).

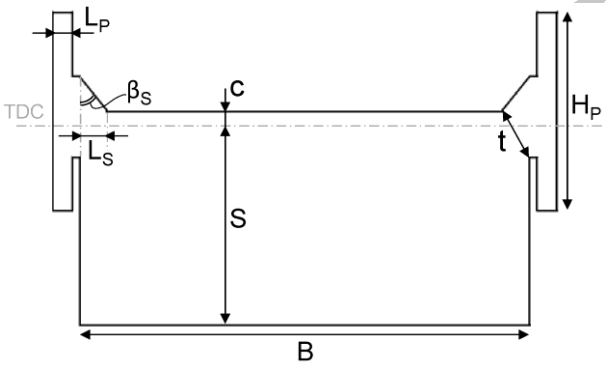

Figure 4 – Relevant dimensions for the 2D representation of the compression chamber.

The length of each porous region, which acts as an equivalent distributed source of pressure loss, is analogous to the actual length of each correspondent component. Each porous coefficient is computed by means of its correspondent flow coefficient, as described in the following section. Finally, inlet and outlet ducts have the same length of suction and discharge nozzles.

3.2 Porous model

The fluid regions of plenums and valves were approximated using a porous medium, where the fluid motion is governed by the Navier–Stokes equations with the addition of a sink term to the momentum equation, in accordance with Darcy's law [21]. In particular, the source term S_i is composed of a viscous loss term and an inertial loss term, generating a pressure drop that is proportional to the velocity and velocity squared, respectively.

$$S_i = -\left(\mu D_{ij} + \frac{1}{2}\rho|V|F_{ij}\right)V \tag{4}$$

where D and F are the Darcy or permeability coefficient and the Forchheimer or resistance coefficient, respectively.

To adequately model a local pressure drop by means of a porous zone it is then sufficient to eliminate the Darcy term and use the Forchheimer term alone, which is proportional to the velocity squared. Considering only the streamwise direction along the porous axis (x-axis), the pressure loss produced by the porous medium is:

$$\Delta p_x = \left(\frac{1}{2} \rho F V_{por}^{\ 2} \right) L_{por} \tag{5}$$

where L_{por} is the length of the porous medium and V_{por} is the mean flow velocity inside the porous region. Since the pressure drop is related to the flow coefficient Ks, a direct correlation can be derived with the resistance loss coefficient. The most common approach is to adopt the incompressible formulation for a localized irreversibility. Considering a reference component (either a valve or a plenum) characterized by its reference cross-sectional area A_{ref}, the pressure drop can be expressed as:

$$\Delta p_x = \frac{1}{2} \rho \left(\frac{1}{Ks} \right)^2 V_{ref}^2 \tag{6}$$

where V_{ref} is the average velocity across the reference area.

By combining Eq. 5 with Eq. 6 it is possible to obtain the equivalent value of the resistance coefficient:

$$F = \frac{1}{L_{por} Ks^2} \left(\frac{V_{ref}}{V_{por}} \right)^2 = \frac{1}{L_{por} Ks^2} \left(\frac{A_{por}}{A_{ref}} \right)^2 \tag{7}$$

where A_{por} is the transverse area of the porous region.

It is apparent that the determination of the resistance coefficient for valves and plenums relies on the knowledge of both flow coefficients (Ks_v and Ks_p). Moreover, they are case dependent, i.e. they need to be recomputed for each different geometrical configuration. The flow coefficients of suction and discharge valves is generally known based on a broad data set coming from experimental tests and is then used as an input parameter for the porous model. Conversely, it is not common to perform experimental tests at the flow bench for suction and discharge plenums. Therefore, their flow coefficients must be computed with CFD steady-state flow simulations according to ref. [10]: the cylinder, together with valves and plenum, is simulated by considering the average mass flow rate of the gases during the whole working cycle. Suction and discharge geometries are simulated separately. Figure 5 shows an example of the resulting flow field for the discharge geometry.

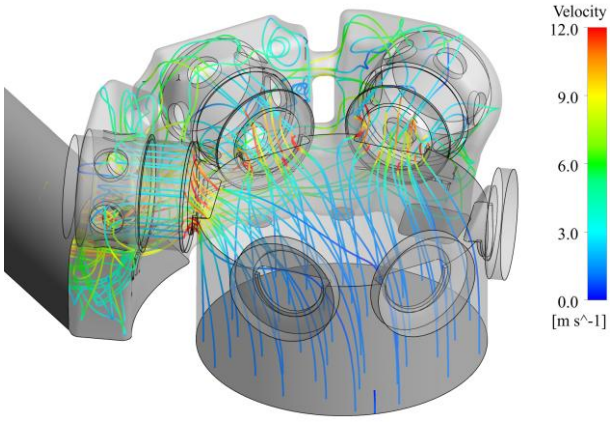

Figure 5 – Results of the 3D CFD steady-state simulations: streamlines in the discharge plenum geometry.

It is important to notice that the porous regions do not introduce any modification in the turbulence quantities and the turbulent kinetic energy is almost constant. Conversely, the

velocity gradients inside the actual geometry of the suction and discharge flow paths are responsible of turbulence generation, and the length scale of turbulent eddies is notably reduced due to the small size of valve's channels. In a previous study [22], some of the authors modified the transport equations for k and ω in the porous region by adding two source terms to account for the turbulence production. A notable improvement of the predictability of the turbulence field was achieved in the 3D steady-state simulations when performing the comparison between the results obtained with the modified porous model and with actual valve. Notwithstanding this, the resulting trend of total pressure was almost equivalent to the simulation with the basic porous model, with just a negligible shift of less than 0.5%. Therefore, the benefits achieved with the enhancement of the porous model definition are not sufficient to justify the increase of the modeling complexity.

3.3 Numerical setup

The time-dependent unsteady Reynolds-averaged Navier–Stokes equations were solved with the commercial code ANSYS® FLUENT® in a two-dimensional form by employing a finite-volume method. As discussed in par. 2 the working fluid was pure nitrogen (N_2), modeled as an ideal compressible gas. The PISO scheme was selected for the treatment of the pressure–velocity coupling. The governing equations were discretized by a second-order upwind scheme for spatial discretization while the turbulence model adopted was the *Standard k-ε* in combination with the enhanced wall treatment for the computation of the boundary layer in the near-wall region. The temporal discretization was obtained using an angular time step of 0.1°.

The compression chamber was discretized by means of a Cartesian grid, featuring 60659 rectangular elements at the Bottom Dead Center (BDC), in order to allow the simulation of the piston motion during the working cycle. The mesh motion was performed by adopting a dynamic layering on the piston, i.e. by adding or removing layers of cells adjacent to the boundary.

The suction and discharge porous mediums used for the modelling of the valves and plenum were meshed using a Cartesian grid of 2825 and 23391 rectangular elements, respectively, while an unstructured grid of 36428 triangular elements was used for the inlet and outlet ducts in order to allow a faster coarsening of the grid. As a result, the total number of elements at BDC is 185947. Due to the piston layering, the number of elements at TDC decreases down to 133262.

A *pressure-inlet* boundary condition is imposed at the inlet of the suction nozzle domain. The values of pressure and temperature measured inside the suction vessels were defined in the model. A *pressure-outlet* boundary condition is imposed at the outlet of the discharge nozzle domain, where only the value of experimental pressure is provided.

Wall boundaries are considered adiabatic since the presence of the cooling system avoids the heat conduction from the hot discharge zone to the suction and compression chambers. The assessment of the thermal state of the compressor cylinder has been extensively discussed by Balduzzi et al. [23]. The results of a conjugate heat transfer (CHT) simulation, validated against experimental measurements, revealed that the fresh gas heating is ranging between 0.4 K and 0.6 K and the metal temperature in the suction zone is almost insensitive to the heating of the discharge zone.

The opening and closing of the suction and discharge valves is automatic and it is regulated by the pressure differences between the compression chamber and the suction and discharge ducts. When a valve is closed, a wall is placed between the pocket and the adjacent porous medium. During the valve opening, the wall condition is substituted with an interface that allows the communication between the porous medium and the fluid region of the

pocket. The valve dynamics can be neglected, since the duration of opening and closing phases is in the order of 1÷2°, due to the low revolution speed.

4. Results

Based on the methodology described above, the working cycle of the head-end of the double-acting cast iron cylinder was simulated and compared to both measured data and numerical predictions of low-order models.

Figure 6 shows the comparison of the experimental in-cylinder pressure with the results of the 2D CFD simplified model. The computed suction and discharge mass flow rates are also reported. The instantaneous values of mass flow rate are in a dimensionless form (m^*), normalized by average mass flow rate per cycle:

$$m^* = \frac{\dot{m}}{\frac{1}{T}\int_0^T \dot{m}(t)dt} \tag{8}$$

Upon examination of the results, some first outcomes become apparent:

- Compression and expansion phases are matching perfectly. This is indeed an important outcome as it testifies the consistency of the modeling approach in evaluating the correct elaborated mass of gas per cycle;
- The pressure trends during the discharge phase are almost superimposed. It is apparent that both the distribution of pressure losses and the gas inertial and dynamic effects are correctly reproduced. In particular, after the valve opening, the inertia of the outflowing gas can be seen from the gradual increase of the discharge mass flow rate, due to the large extent of the compression chamber. As a result, the piston keeps compressing the gas up to 20% above the value in the discharge ambient even if the discharge valve is already open.
- The computed pressure during the suction phase is higher than the measured values. This behavior is probably due to an underestimation of the pressure losses. Notwithstanding this, the pressure values at the BDC are matching, denoting an analogous volume filling.

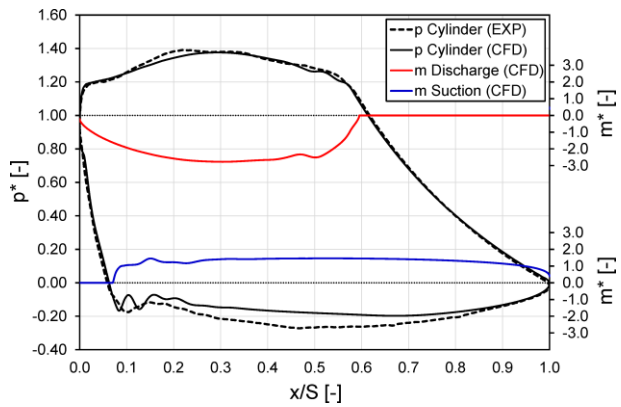

Figure 6 – Comparison between computed and measured in-cylinder pressure; computed suction and discharge mass flow rate profiles.

Focusing the attention on the matching between pressure trends during the suction and discharge phases, Figure 7 and Figure 8 show the instantaneous pressure as a function of the

piston position considering the discharge and suction sensors, respectively. The comparison between measured and computed values is carried out for the cylinder head, the valves and the nozzles sensors.

From a perusal of both figures, one can readily notice that the global amplitude and the phasing of pressure oscillations are comparable. In particular, the discharge wave reaches the valve and nozzle sensors at the correct time, then the trends of increasing pressure have analogous slopes and the maximum overpressure is correctly predicted in terms of both position and magnitude.

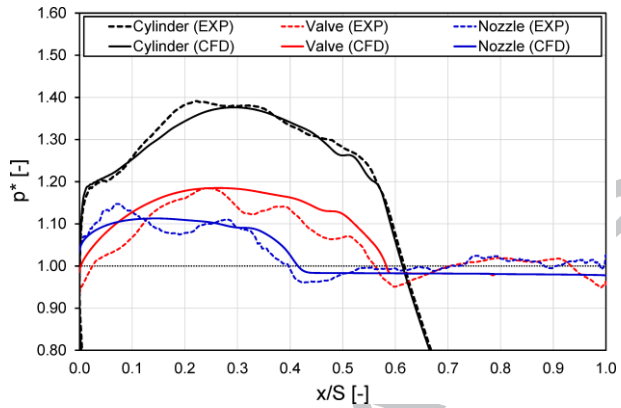

Figure 7 – Comparison between computed and measured pressure during the discharge phase at three locations: cylinder head, discharge valve head and discharge nozzle.

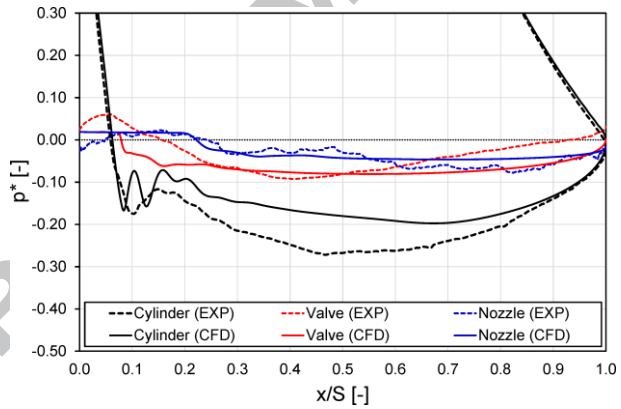

Figure 8 – Comparison between computed and measured pressure during the suction phase at three locations: cylinder head, suction valve head and suction nozzle.

The difference lies in the presence of high-frequency fluctuations in the experimental data due to reflections of the pressure waves along the components of the gas chamber. The presence of valve cages, bend ducts and T-junctions is indeed ignored in the simplified 2D geometry and only their primary effect is introduced through a distribute source of pressure loss. Wave reflections inside these components represent a secondary effect that is less significant for the p-V cycle prediction.

To better clarify some of the phenomena described in the analysis of the compression cycle, Figure 9 and Figure 10 show the contours of pressure and the flow streamlines in the cylinder and the discharge line at two different crank-angle (ϑ) positions. In particular, Figure 9 refers to ϑ=266°CA, corresponding to few degrees after the discharge valve opening ($x/S\approx0.6$). The pressure wave traveling along the plenum volume is clearly visible, as well as the "advancing front" of discharge gases. Focusing on the cylinder volume, a non-uniformity of the pressure distribution is apparent. This latter phenomenon is related to the inertia of the outflowing gas, as illustrated by the streamlines: only the portion of gas close in proximity of

the discharge pocket is starting the discharge process, while the largest amount of volume is "undisturbed", therefore is still experiencing the compression.

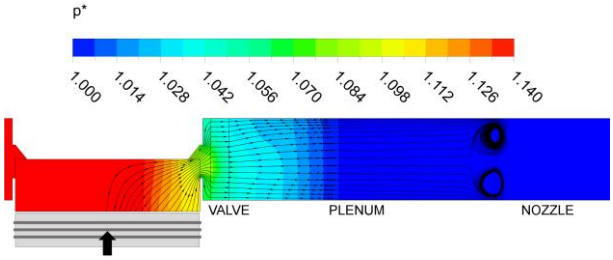

Figure 9 – Discharge phase @266°CA: pressure contours and flow streamlines.

Figure 10 refers to ϑ=300°CA, corresponding to the position where the cycle reaches the maximum pressure (x/S≈0.3). In this condition, the discharge flow is experiencing the maximum pressure drop and the distribution of the losses can be easily observed. As expected, the largest drop is localized inside the porous medium of the valve, representing roughly half of the global loss (~48%). It is apparent that the valve pocket and the gas plenum have a strong impact on the irreversibilities associated with viscous friction, since they contribute to ~23% and ~29% of the global loss, respectively. Therefore, an accurate prediction of their losses and a suitable representation of their fluid-dynamic response are pivotal to correctly account for all of the effect that contribute to the gas exchange process of the machine.

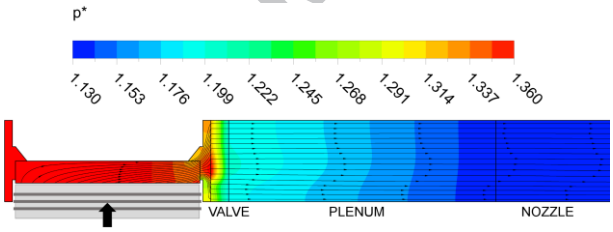

Figure 10 – Discharge phase @300°CA: pressure contours and flow streamlines.

The results of the 2D CFD simulations were finally compared with the results obtained on the same test case with low-order numerical models reported in ref. [20]. Figure 11 reports the predictions of the pressure inside the cylinder of a lumped parameter model (0D) and a one-dimensional FVM model. In the latter, the 1D discretization of the compression chamber is applied in the valve-to-valve direction.

The lumped parameter model underestimates the absorbed work, since the predicted pressure is higher than the measured pressure during the suction phase and lower during the discharge phase. In particular, the deviation from the experimental curve occurs at the angular positions of valves opening: the 0D approach does not allow to account for the inertial effect of the mass flowing in and out the compression chamber. It is possible to clarify this behavior focusing on the discharge phase: the pressure variation inside the cylinder at each step depends on both the amount of mass flowing out from the cylinder and the volume reduction. Since the volume reduction is the same for all of the models, the lower in-cylinder pressure predicted by the 0D model is due to a higher mass flow rate after the valve's opening. The mass flow rate depends on the flow coefficients, which are the same for all of the models, and on the pressure difference between cylinder and discharge plenum. Thanks to the volume discretization, the 1D and 2D models evaluate the local pressure difference across the throat section, while the 0D model performs the calculation with averaged values. The local reduction of pressure shown in Figure 9, which delays the

discharge of gas, is not accounted for in the 0D model, thus leading to a faster discharge process.

On the contrary, the FVM model is able to correctly reproduce the pressure increase after the discharge valve opening and the pressure reduction after the suction valve opening. A satisfactory matching can be observed with the experimental trend during the suction phase, while the pressure is overestimated during the discharge phase.

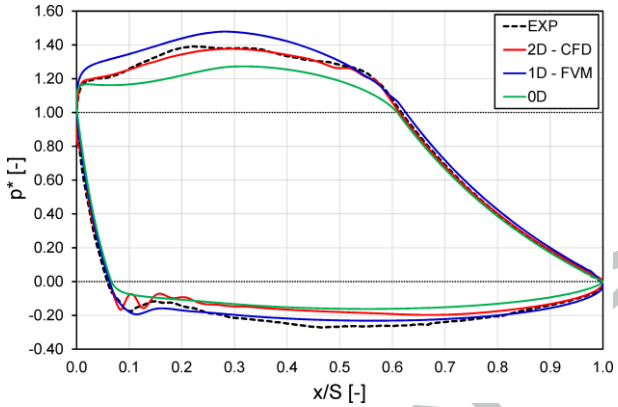

Figure 11 – In-cylinder pressure: comparison between measured values and results of different numerical approaches.

To quantify the accuracy and reliability of the numerical models, the prediction capability of the compressor performance was finally assessed in terms of both the indicated absorbed power and the matching between p-V cycles. The first was evaluated by calculating the absolute error in the predicted power between the numerical models and the experimental measurements. The latter was addressed making use of the coefficient of determination R^2 [24], here defined as:

$$R^2 = 1 - \frac{\sum_{\vartheta=0°}^{360°} (p_{NUM}(\vartheta) - p_{EXP}(\vartheta))^2}{\sum_{\vartheta=0°}^{360°} (p_{NUM}(\vartheta) - p_{EXP,ave})^2} \qquad (9)$$

The experimental pressure was selected as the reference data to which the pressure variations of numerical models can be compared and $p_{EXP,ave}$ represents the average pressure over a revolution of the crank-shaft.

Figure 12 shows the values of the two parameters for all of the three analyzed numerical models. As expected, the lumped parameter model is considerably worse than the other approaches since it does not allow to compute the compressor performance with an adequate accuracy. A power difference of about 13% was estimated and the matching between the in-cylinder pressure cycles is the poorest since the R^2 is lower than 98.5%. The 2D CFD model provides the best estimate of the trend of the pressure profile (R^2=99.6%) although in terms of aggregate parameter is slightly worse than the FVM model, with an error in the absorbed power of 4.7%.

Concerning the calculation time, low order models are very fast if compared to CFD models. Indeed, 0D and 1D models have a time scale of few seconds to achieve convergence. Conversely, a 2D simulation has a time scale of few hours for a single run, while the simulation time for a full 3D run is estimated in 4÷6 days.

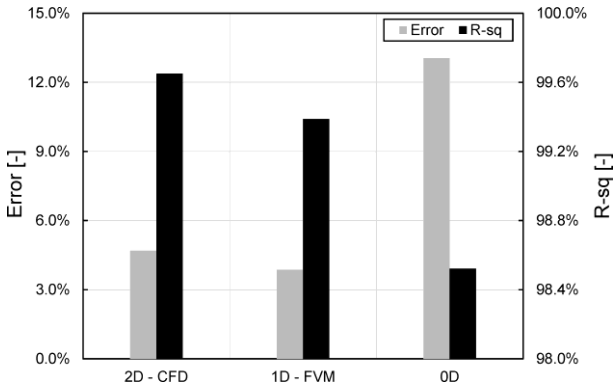

Figure 12 – Error in the prediction of the absorbed power and coefficient of determination: comparison between different numerical approaches.

5. Modelling strategies

An extended sensitivity analysis for the assessment of the proper simplifications required to allow the reduction of the three-dimensional fluid domain to an equivalent two-dimensional representation was carried out in a preliminary stage. Different configurations were tested by varying the compression chamber geometry, the pocket simplification and the porous mediums definition and extension. In the present paragraph, the results of some preliminary choices are shown, aimed at highlighting the effect of some critical features for an accurate two-dimensional simulation of a reciprocating compressor. In particular, the authors selected three alternative geometrical configurations, which differ from the *baseline* configuration. The aim is to analyze the most important aspects of the proposed approach in order to differentiate between influential and non-influential characteristics, with respect to the results described in the previous paragraph. It is worth pointing out that all of the investigated features directly affect the accuracy of the final and have a mutual influence between themselves; the analysis tried to decouple the effects of each choice and to highlight their impact on the simulation outcomes.

Configuration 1

Concerning the modelling of the valve pockets, the results of a more simplified geometry are reported to assess the required detail level of the pocket shape to adequately predict the pocket losses. Figure 13 shows the computational domain of the analyzed configuration where a basic rectangular shape was used, therefore neglecting the actual shape of the pocket window and the machining on the head. With respect to the *baseline* geometry, the pocket length (L_P) is increased in order to guarantee the same dead volume and the masking height is not modified.

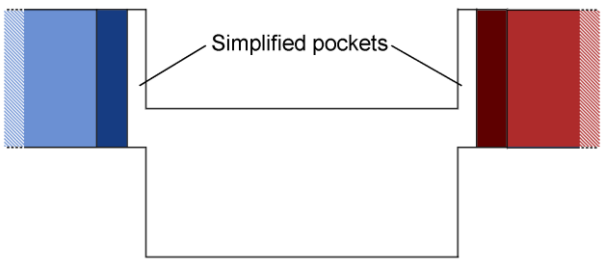

Figure 13 – Computational domain of the Configuration 1 with simplified pocket shape.

Configuration 2

In order to evaluate the influence of the porous mediums modelling, a simplified configuration that uses a single porous medium for modelling the pressure losses of valve and plenum is analyzed, as shown in Figure 14. In the *baseline* configuration the valve loss and the plenum loss were modeled separately using two different flow coefficients for each phase, acting as two equivalent distributed sources of pressure loss. The new combined porous medium length is calculated considering the sum of the valve and plenum length while the global resistance coefficient F is computed in order to obtain the analogous global pressure drop of valve and plenum, as reported in Eq. 10:

$$F = \frac{1}{(L_{valve} + L_{plenum}) \cdot Ks_{valve+plenum}^{\ 2}} \left(\frac{A_{por}}{A_{ref}} \right)^2 \tag{10}$$

The cylinder geometry is not modified with respect to the *baseline* configuration.

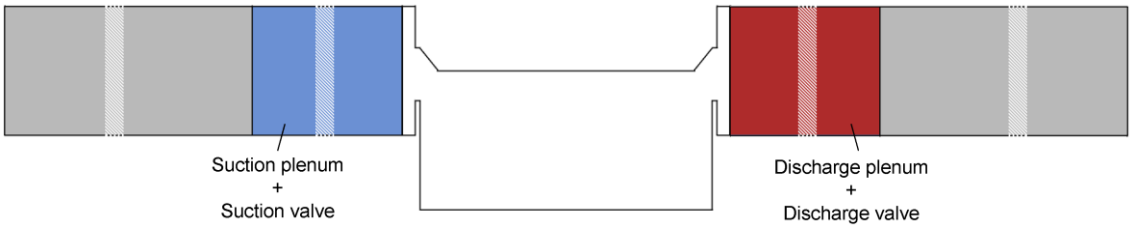

Figure 14 – Computational domain of the Configuration 2 with combined porous mediums.

Configuration 3

Finally, to examine the effect of fine details of the compression chamber geometry on the response of the model, a different strategy for the definition of the two critical cross-section of the pockets is analyzed. In place of the imposition of the equivalence of the pocket throat t, as proposed in Eq. 3, the pocket shape is defined by maintaining the same masking height H_m of the 3D geometry, as shown in Figure 15. This implies that, conversely to the *baseline* configuration, the piston starts the masking of the windows of the valve pockets at the correct angular position. On the other hand, the 2D throat section t increases, not being anymore consistent with the ratio between the actual throat area and the piston surface of the 3D geometry.

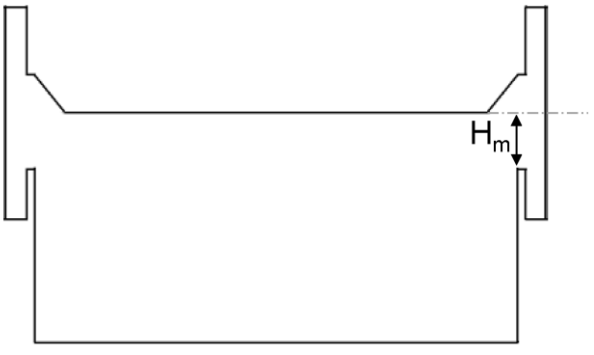

Figure 15 – Computational domain of the Configuration 3 with corrected masking height.

On these bases, a comparative analysis was carried out between the selected configurations with the goal of establishing the sensitivity of the compression cycle to the modified characteristics. Figure 16 reports the comparison of the experimental in-cylinder pressure with the results of all of the four 2D CFD numerical configurations. The following observations can be made:

- The results of *configuration 1* reveal a substantial modification of the working cycle with respect to the *baseline*. In particular, a large increase of pressure drops during both the suction and discharge phases can be observed. As a consequence, the pressure trend during the compression phase is not matching anymore with the experiments. Therefore, the model is not able to predict the correct elaborated mass of gas per cycle;
- The results of *configuration 2* reveal a slight modification of the dynamic response, in particular during the discharge phase. Globally, the working cycle is not significantly affected when considering a single "combined" porous medium, although the in-cylinder pressure is moderately underestimated in the first part of the discharge and overestimated when getting closer to the TDC;
- The results of *configuration 3* reveal an almost equivalent behavior with respect to the *baseline* configuration.

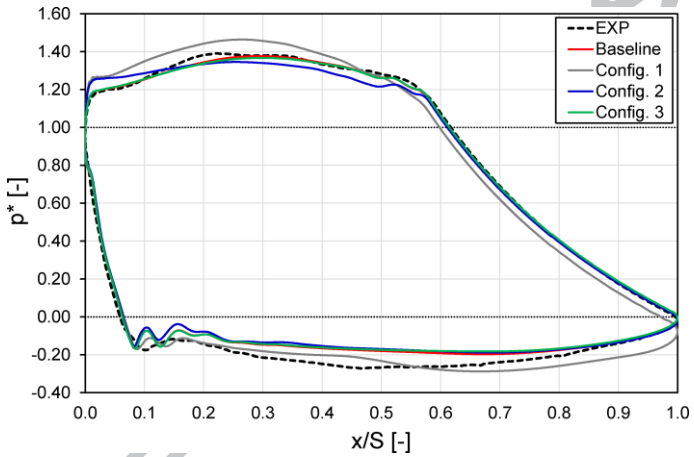

Figure 16 – In-cylinder pressure: comparison between measurements and results of four numerical models.

Within these considerations, the analysis was further examined in depth by focusing on a more detailed evaluation of the pressure trends during the suction and discharge processes. Figure 17 and Figure 18 report the same comparisons of Figure 16 showing the zooms of the high pressure and low pressure phases of the cycle, respectively. In this way, the small-scale differences can be appreciated, especially for *configuration 2* and *configuration 3*, which were still in good agreement with the experimental data.

Starting from *configuration 2*, the change in the porosity distribution along the suction and discharge lines affects the outflow of gas at the time of valve opening. Indeed, the phenomenon of pressure increase with discharge valves already open, observed experimentally and also numerically with the *baseline* model, is interrupted in advance. This leads to a subsequent lower pressure during the largest part of the discharge phase.

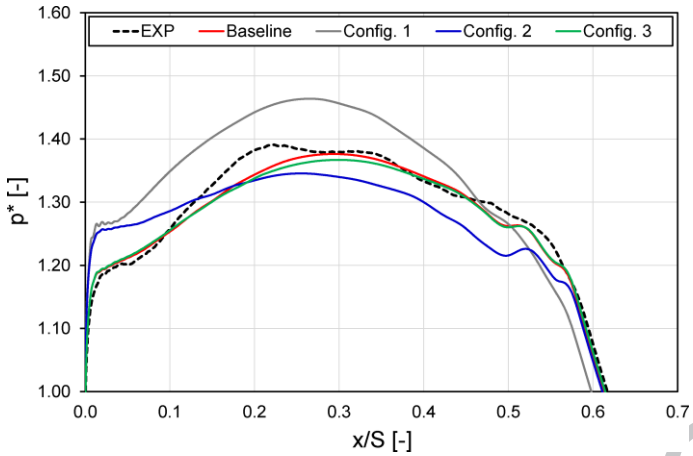

Figure 17 – In-cylinder pressure during the discharge phase.

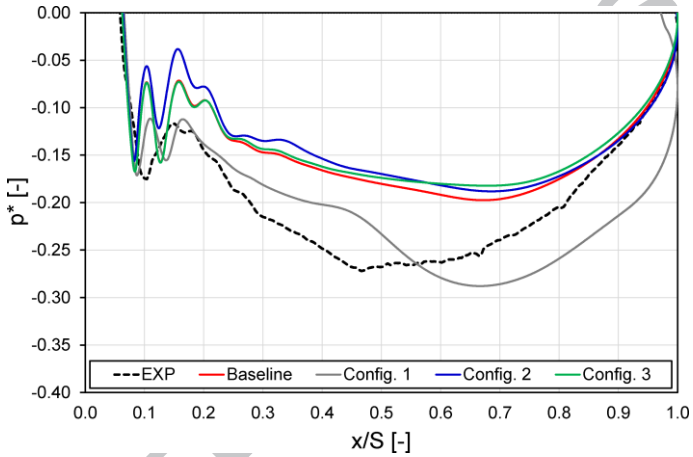

Figure 18 – In-cylinder pressure during the suction phase.

To analyze this inconsistency, Figure 19 reports the pressure contours and the flow streamlines in the cylinder and the discharge line at ϑ=300°CA. The whole porous medium representing both valve and plenum is characterized by an almost linear decrease of pressure, conversely to Figure 10 for the *baseline* configuration, in which a strong decrease of pressure is concentrated in a short length corresponding to the valve. Although the global resistance of the two modeling approaches is analogous, the splitting of the two contributions is necessary to provide the correct resistance to the flow in correspondence of the exact distance from the cylinder.

Moving to *configuration 3*, an almost negligible variation of pressure levels reached during the suction and discharge phases can be detected. This is related to the minimal increase of the throat section when changing the masking height, which leads to a reduction of the pocket losses. With particular reference to the suction phase, the prediction is slightly worsened.

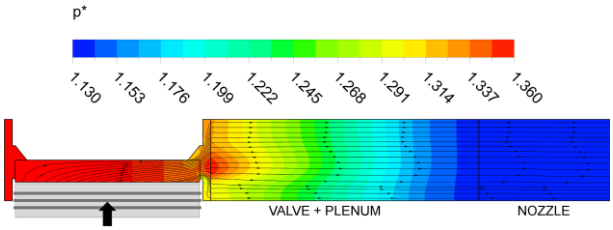

Figure 19 – Pressure contours and flow streamlines for the Configuration 2: discharge phase @300°CA.

The attention was then focused on the comparison between the propagation of pressure waves in the suction and discharge lines. Figure 20 and Figure 21 show the experimental and numerical pressure oscillations in correspondence to valve heads and nozzles for the discharge system and suction system, respectively. From a perusal of both figures it can be easily seen that the effect of the modeling strategy of cylinder and porous mediums has a minor impact of the fluid-dynamic response of the ambient external to the cylinder. In particular, the pressure at both discharge (Figure 20 (b)) and suction (Figure 21 (b)) nozzles is almost unaffected, since the curves for all of the tested configurations are almost superimposed.

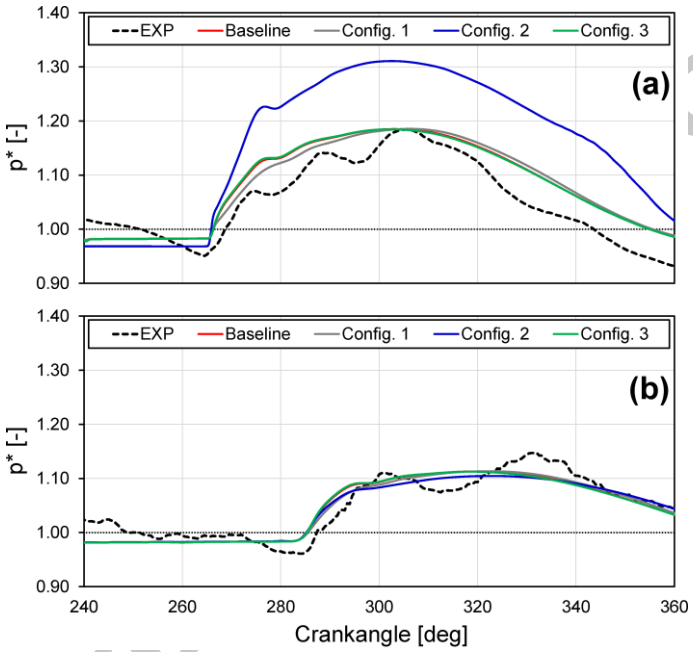

Figure 20 – Comparison between computed and measured pressure during the discharge phase at two locations: discharge valve head (a) and discharge nozzle (b).

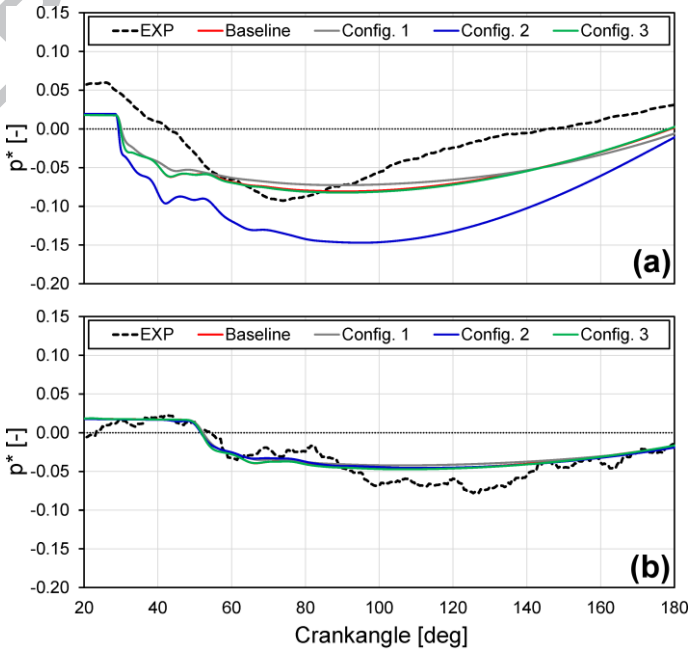

Figure 21 – Comparison between computed and measured pressure during the suction phase at two locations: suction valve head (a) and suction nozzle (b).

Also the pressure at both discharge (Figure 20 (a)) and suction (Figure 21 (a)) valve heads is almost unaffected, with the exception of *configuration 2*. This behavior is simply related to the fact that with the combined porous medium there is no distinction between valve and plenum, therefore is not possible to define a location where placing the sensor for the valve head. In other words, the difference is due to an intrinsic limitation of such porous modeling and it does not affect the results of the simulation.

The last analysis was addressed to quantify the different prediction capability of the tested configurations by the evaluation of the matching with the experimental p-V cycle. The results in terms of coefficient of determination are illustrated in Figure 22.

As expected, *configuration 1* is characterized by the lowest similarity with the measured data. Based on this evidence, it is clear that a suitable 2D model must include some critical features of the valve pocket in order to define an equivalent geometry. This requirement is due to the substantial influence of pocket losses on the compressor performance. A better estimate of the trend of the pressure profile is provided by *configuration 2*, although the matching is still worse than the *baseline*. The correct distribution of sources of loss is pivotal to properly simulate the resistance offered to the flow and, therefore, the mass transport. Only *configuration 3* shows a R^2 almost analogous to the *baseline* configuration. This implies that the level of geometrical detail reached is sufficient and such a small modification does not affect the model response.

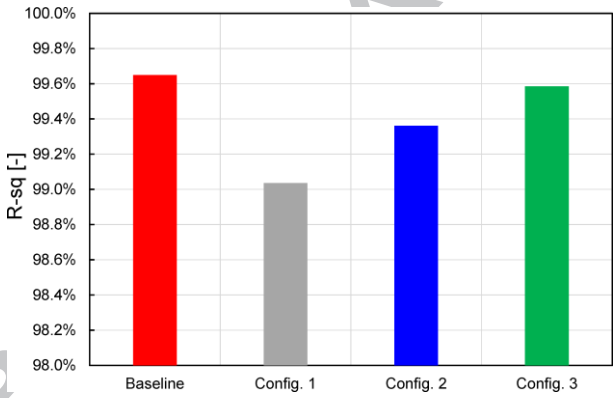

Figure 22 – Coefficient of determination: comparison between different geometrical configurations.

7. Conclusions

In this paper, an original CFD numerical approach aimed to predict the working cycle of a large-bore reciprocating compressor has been presented. The method is based on a two-dimensional simplification of the computational domain and on the replacement of the valve and plenum geometries by equivalent porous regions. The goal of both simplifications is to allow a remarkable reduction of the computational resources required for the transient simulation of the machine. Three-dimensional CFD simulations for similar systems are in fact limited by the large size of the mesh resulting from the extent of the computational fluid domain. In addition, the automatic valve would require a special treatment due to the complexity of the inner geometry and to the dynamic motion of valve rings.

This method has been applied to the simulation of a real-world application (double-acting cast iron cylinder) in order to verify its prediction capability. The tested compressor was equipped with multiple sensors in order to collect field data for the validation of the method itself. The comparison of the results of the unsteady CFD simulation of the compressor cycle demonstrated the accuracy of the proposed tool in predicting the compressor performance, showing a significant reduction of the error in the cycle estimation with respect to corresponding 0D and 1D numerical models.

The reduction of the three-dimensional fluid domain to an equivalent two-dimensional representation relies on some assumptions that were made by the authors. Once the method was validated, the results of three modified versions were presented to identify some of the critical features of the 2D geometry that affect the accuracy of the model. The sensitivity analysis led to the following indications:

- A high level of detail in the definition of the pocket shape is needed to properly account for the pocket losses on the compressor performance;
- Valves and plenums must be modeled as distinct sources of loss through dedicated porous mediums to correctly distribute the resistances to the flow along the gas flow path.

Due to the cost-efficiency of the process, compared to the fully 3D unsteady CFD simulation of the compressor cycle, and to the possibility of an easy implementation of the model in a general purpose CFD code without any programming effort, it turns out to be an accurate yet practical tool that can be used during all phases of the system development. Indeed, this method allows the simulation of the compressor within timescales consistent with the necessity of the design stage, similar to low order models, though guaranteeing the accuracy of a high-fidelity simulation.

Acknowledgements

Thanks are due to Prof. Ennio Antonio Carnevale of the Università degli Studi di Firenze for supporting this research activity.

References

[1] R. Traversari, A. Rossi, M. Faretra, Thermo-fluid-dynamic design of Reciprocating Compressor Cylinders by Fluid Structure Interaction (FSI), Proc. of the ASME PVP Conference, Baltimore, Maryland, United States, 2011.

[2] E.L.L. Pereira, C.J. Deschamps, Influence of piston on effective areas of reed-type valves of small reciprocating compressors, HVAC&R Research, 17(2) (2011) 218–230, doi:10.1080/10789669.2011.566463.

[3] M. Costagliola, The theory of spring-loaded valves for reciprocating compressors, Journal of Applied Mechanics, 1950, pp. 415-420.

[4] E. Winandy, O.C. Saavedra, J. Lebrun, Simplified modeling of an open-type reciprocating compressor, Int. J. of Thermal Science, 41 (2002) 183-192.

[5] M. Elhaj, F. Gu, A.D. Ball, A. Albarbar, M. Al-Qattan, A. Naid, Numerical simulation and experimental study of a two-stage reciprocating compressor for condition monitoring, Mechanical Systems and Signal Processing, 22 (2008) 374-389.

[6] B. Yang, C.R. Bradshaw, A.A. Groll, Modeling of a semi-hermetic CO2 reciprocating compressor including lubrication submodels for piston rings and bearings, Int. J. of Refrigeration, 36 (2013) 1925-1937.

[7] F. Bauer, Valve Losses in Reciprocating Compressors, Int. Compressor Engineering Conf., Purdue University, Indiana, 1988.

[8] L. Boeswirth, V. Milovanova, Simple but Efficient Methods for Estimation of Value Loss, Capacity Loss Due to Suction Valve Throttling and Heat Transfer in Cylinder, Int. Compressor Engineering Conf., Purdue University, Indiana, 1998.

[9] E.H. Machu, Problems with modern high speed short stroke reciprocating compressors: Increased power requirement due to pocket losses, piston masking and gas inertia, eccentric gas load on the piston, Proceedings of Gas machinery conference USA, 1998.

[10] F. Balduzzi, G. Ferrara, A. Babbini, G. Pratelli, CFD evaluation of the pressure losses in a reciprocating compressor: a flexible approach, ASME 11th ESDA Conference, Nantes, France, 2012.

[11] F. Balduzzi, G. Ferrara, R. Maleci, A. Babbini, G. Pratelli, A Parametric Computational Fluid Dynamics Analysis of the Valve Pocket Losses in Reciprocating Compressors, Journal of Pressure Vessels Technology, 137(1) (2015) 1-10, doi: 10.1115/1.4027660.

[12] I. Stiaccini, G. Galoppi, F. Balduzzi, M. Sacco, S. Santoni, G. Ferrara, Analysis of valve-retainer orientation influence on a reciprocating compressor for natural gas vehicle refueling stations, Journal of Natural Gas Science and Engineering, 38 (2017) 516-526, doi:10.1016/j.jngse.2016.12.035.

[13] I. Stiaccini, L. Romani, L. Ferrari, G. Ferrara, A Hybrid Time-frequency Domain Approach for Numerical Modeling of Reciprocating Compressors, 81 (2015) 1102-1112, doi:10.1016/j.egypro.2015.12.132.

[14] I. Stiaccini, G. Galoppi, L. Ferrari, G. Ferrara, A reciprocating compressor hybrid model with acoustic FEM characterization, 63 (2016) 171-183, doi:10.1016/j.ijrefrig.2015.10.036.

[15] A. Gimelli, A. Rapicano, F. Barba, O. Pennacchia, Reciprocating Compressor 1D Thermofluid Dynamic Simulation: Problems and Comparison with Experimental Data, International Journal of Rotating Machinery, Volume 2012, Article ID 564275, 13 pages, doi:10.1155/2012/564275.

[16] E.H. Machu, Increased Power Consumption of High-Speed, Short -Stroke Reciprocating Compressors Caused by Pocket Losses and Gas Inertia Effects, Compressor Tech, March-April, 1999, pp. 107-111.

[17] G. Machu, Calculating reliable impact valve velocity by mapping instantaneous flow in a reciprocating compressor. Proceedings of gas machinery conference GMRC USA, 2004.

[18] G. Machu, Pulsationen im Verdichtungsraum - eine potentielle Schadensursache, Industriepunpen und Kompressoren Heft 2/2005 Vulkann Verlag Essen, 2005.

[19] R. Aigner, Internal flow and valve dynamics in a reciprocating compressor, PhD Thesis, Wien, 2007.

[20] I. Stiaccini, N. Fiorini, F. Balduzzi, G. Ferrara, A. Babbini, G. Orsi, Large size reciprocating compressor analysis with a Finite Volume 1D model, Proc. of the 10th EFRC Conference, Düsseldorf, Germany, September 14-15, 2016.

[21] S. L. Lee, J. H. Yang, Modeling of Darcy-Forchheimer Drag for Fluid Flow Across a Bank of Circular Cylinders, Int. J. Heat Mass Transfer, 40(13) (1997) 3149-3155.

[22] F. Balduzzi, Development of a CFD approach for the performance prediction of reciprocating compressors, PhD Thesis, Firenze, 2012.

[23] F. Balduzzi, A. Tanganelli, G. Ferrara, A. Babbini, R. Maleci, Numerical analysis and experimental assessment of the cylinder temperature in a reciprocating compressor, Proc. of the ASME PVP Conference, Boston, Massachusetts, USA, 2015, doi:10.1115/PVP2015-45574.

[24] J. Mandel, The statistical analysis of experimental data, Dover Publications, New York, 1984.